Springer

Journal of
Mechanical
Science and
Technology

Journal of Mechanical Science and Technology 22 (2008) 1222~1229

www.springerlink.com/content/1738-494x

Wave overtopping simulations over coastal structures

Jong-Chun Park[1,*], Byung-Hyuk Lee[1] and Key-Yong Hong[2]

[1]*Dept. of NAOE, Pusan National University 30 Jangjeon-dong, Geumjeong-gu, Busan, Korea*

[2]*Ocean Engineering Research Department, MOERI, KORDI 171 Jang-Dong, Yuseong-Gu, Daejeon, Korea*

(Manuscript Received October 17, 2007; Revised March 4, 2008; Accepted March 7, 2008)

Abstract

A large-eddy simulation (LES) model has been developed to investigate nonlinear wave run-up and overtopping. The Navier-Stokes equations are solved by using a finite differential algorithm, and the modified Marker-Density Function (MDF) technique (Miyata and Park, 1995) is employed for solving nonlinear free-surface motions. In order to evaluate the present model, three numerical simulations are presented: solitary wave run-up on a vertical wall, flow over a broad-crested weir, and regular waves overtopping a sloping seawall. The results are compared with data from experiments and other numerical models.

Keywords: Wave run-up; Overtopping; Large-eddy simulation (LES); Non-linear free-surface motions

1. Introduction

The estimation of wave overtopping is a key aspect of the design of coastal structures. Indeed, the failure of many seawalls has been attributed to wave overtopping. The water released after an overtopping event also contributes to coastal flooding. Overtopping is hydrodynamically complicated as the waves impact and run-up a coastal structure, until the crest level of the structure is exceeded by the maximum run-up. For breaking waves, there is a further complication due to turbulence production and related energy dissipation in the form of heat.

During the past 50 years, researchers have developed many numerical methods to investigate wave overtopping over coastal structures. However, the rate of progress of model development has been relatively slow because of the complexity of the turbulent free surface flows involved. Numerical models of wave overtopping may be classified according to whether they are based on the depth-averaged Navier-Stokes equations, or Reynolds-averaged Navier-Stokes equations (RANS). The former include both the shallow water equations and Boussinesq-type equations (see, e.g., [1-7]). In these models, breaking wave energy dissipation is incorporated through simple dissipative terms in the equations. The RANS solvers generally utilize a surface capturing method, such as the Volume-of-Fluid (VOF) technique of Hirt and Nichols [8], to represent the non-linear free surface motions (see, e.g., [9-14]). In the RANS solver, turbulent fluctuations on the mean flow are represented by the Reynolds stress terms.

The present study describes the use of large-eddy simulation (LES) with a sub-grid scale (SGS) turbulence model to investigate non-linear wave run-up and overtopping. The Navier-Stokes equations are solved by using a finite differential algorithm, and the modified Marker-Density Function (MDF) technique [15] is employed for solving nonlinear free-surface motions. Waves are generated from a numerical wave-maker installed at the inflow boundary of the computational domain. To verify the model, the benchmark case of solitary wave run-up at a vertical wall is simulated, and the results compared against published experimental data and predictions by alternative numerical schemes. Further results are pre-

*Corresponding author. Tel.: +82 51 510 2480, Fax.: +82 51 583 2485
E-mail address: jcpark@pnu.ehu
DOI 10.1007/s12206-008-0304-1

sented for open channel flow over a broad-crested weir. Finally, regular wave overtopping of a sloping seawall with seaward face of slope 1:3 is investigated.

2. Numerical model

2.1 Governing equations

After applying the filtering operation to the momentum equations and the continuity equation, we get the following equations for the filtered field.

$$\frac{\partial u_i}{\partial t} = -\frac{\partial (u_i u_j)}{\partial x_j} - \frac{\partial p}{\partial x_i} + \frac{\partial}{\partial x_j}\left(-\tau_{ij} + 2\nu S_{ij}\right) + f_i \tag{1}$$

$$\frac{\partial u_i}{\partial x_i} = 0 \tag{2}$$

where, u_i indicates the velocity vector, t the time, x_i the coordinates, p the pressure, ν the viscosity, f_i the external forces including the gravitational acceleration, and S_{ij} the SG components of the deformed velocity tensor as follows:

$$S_{ij} = \left(\frac{\partial u_i}{\partial x_j} + \frac{\partial u_j}{\partial x_i} \right) \tag{3}$$

and, τ_{ij} is referred to as the sub-grid scale (SGS) stress tensor in the LES, and must be modeled in terms of the resolved scale velocity, u_i, in order to obtain a closure for Eq. (1).

Several closure models for the SGS stress have been proposed. They fall into one of the following general categories: eddy viscosity models, scale similarity models, mixed models and the Lagrangian-based models. The Smagorinski model [16] is the most basic model in LES, and the assumption for the eddy viscosity ν_S is derived as

$$\tau_{ij} = -2L_S^2 \left|\bar{S}_{ij}\right| \bar{S}_{ij} \tag{4}$$

$$S_{ij} = \frac{1}{2}\left(\frac{\partial u_i}{\partial x_j} + \frac{\partial u_j}{\partial x_i} \right) \tag{5}$$

where, S_{ij} is the strain rate tensor defined as

$$\left|S_{ij}\right|^2 = 2S_{ij}^2 \tag{6}$$

And the length scale, L_S, is set at the minimum value among the grid size and the minimum spacing, as noted by Takakura et al. [17]:

$$L_S = \min\left[C_S \Delta, C_T \left(\Delta x_1, \Delta x_2, \Delta x_3 \right) \right] \tag{7}$$

$$\Delta = \sqrt[3]{V} \tag{8}$$

Here, V is the volume of a cell; Smagorinsky's coefficient, C_S, is set at 0.1, and Takakura's coefficient, C_T, set at 1.0.

By implementing the conservation laws with these equations, the solution is achieved using the modified Marker-And-Cell (MAC)-type time-marching algorithm [18].

2.2 Treatment of nonlinear free-surface motions

The configuration of the interface is determined by applying the fully nonlinear free-surface condition. At the free surface, the following fully nonlinear kinematic and dynamic conditions can be applied while neglecting the viscous stress and surface tension:

$$\frac{\partial M_\rho}{\partial t} + \mathbf{u} \cdot \nabla M_\rho = 0 \tag{9}$$

$$p = 0 \tag{10}$$

where the MDF, M_ρ, takes a value between 0 and 1 all over the computational domain. Eq. (9) is calculated at each time step and the free-surface location is determined to be a point where the MDF takes the mean value as

$$\bar{M}_\rho = \frac{1}{2} \tag{11}$$

In the present study, in order to prevent excessive numerical diffusion in the vicinity of the interface, we do not directly solve Eq. (9), but instead solve Eq. (12) by introducing both the *mapping function* and the *re-distribution algorithm* [19] to the previous MDF technique [15]. As a mapping function, the distance function, ϕ, is employed in Eq. (9) and defined continuously in the whole domain of the simulation.

$$\frac{\partial \phi}{\partial t} + u\frac{\partial \phi}{\partial x} + v\frac{\partial \phi}{\partial y} + w\frac{\partial \phi}{\partial z} = 0 \tag{12}$$

Then, the distribution of the MDF at each time step is updated by maintaining the interface location as

$$M_\rho = \begin{cases} M_\rho^1 & \text{if } \phi > \varepsilon_0 \\ M_\rho^2 & \text{if } \phi < -\varepsilon_0 \\ \bar{M}_\rho + \tilde{M}_\rho \cdot \left(\phi/\varepsilon_0\right) & \text{otherwise} \end{cases} \tag{13}$$

where, $\tilde{M}_\rho = \left(M_\rho^1 - M_\rho^2\right)/2$ and $\varepsilon_0 = 2\left(\Delta x\right)_{\min}$.

Eq. (12) is solved for using the fourth-order Runge-Kutta scheme for time integration and the third order MUSCL scheme for the convection term.

On the other hand, the dynamic free-surface

condition of Eq. (10) is implemented by the so-called "irregular star" technique [20] in the solution process of the Poisson equation for the pressure. In free-surface problems, it is very important to extrapolate the physical values onto the free-surface, so the pressure on it is determined by extrapolating from the neighboring fluid to the free-surface location. The pressures are extrapolated with zero gradient in the approximately normal direction to the free surface, while the static pressure difference in the vertical direction, due to the gravity, is taken into consideration. Similarly, the velocities are extrapolated at the interface with approximately no normal gradient from the fluid region. This treatment roughly accords with the viscous tangential condition at the free-surface.

2.3 Numerical schemes

The numerical scheme for the convective terms in Eq. (1) must be carefully chosen, since it often renders decisive influences on the results. In the present model, a flux-split method with a variable mesh size, which is like a third-order MUSCL scheme, is employed so that variable mesh system can be used for all three directions. A second-order-centered scheme is employed for the diffusive terms, and the second-order Adams-Bashforth method is used for time integration.

2.4 Boundary conditions

At the inflow boundary of the computational domain, a numerical wavemaker is established by prescribing the inflow velocities based on the water particle velocities of the linear wave (or Stokes second-order wave), which is like a flexible flap wavemaker. In the present simulation, the bathymetry is approximated in a step-like shape for simplicity, and a no-slip boundary condition imposed at solid walls.

3. Numerical simulation

3.1 Solitary wave run-up on a vertical wall with a beach slope

First, to generate a solitary wave, a piston-type wave maker is assumed, and the displacement and velocity of wave paddle movements are given at the inflow boundary as follows:

$$\xi_{(cm)} = A_1 \tanh\left[A_2\left(t-258\right)-A_3\right]-A_4 \tag{14}$$

$$u_{(cm)} = A_1 A_2 \operatorname{sech}^2\left[A_2\left(t-258\right)-A_3\right] \tag{15}$$

where, the coefficients A_1 , A_2 , A_3 and A_4 in the above Eqs. (14)-(15) are set as Table 1.

Table 1. Solitary wave parameter.

A_1	A_2	A_3	A_4
11.31	1.51	3.735	0.0347

The simulated wave profile is compared with the experiments [21], and Boussinesq's equation of solitary waves, as shown in Fig. 1. The present result agreed well with the experiments and the theoretical approximation, and that means the present wave making technique is proper to generate a soliton.

Next, the series of 2-D flume experiments for solitary wave propagation and run-up on a vertical wall with a beach slope, which were conducted by Briggs et al. [22], are reproduced in the present 2-D numerical wave flume. Fig. 2 shows a schematic view of the 2-D wave flume and the location of wave gauges. The compound-slope, fixed-bed bathymetry consisted of three different slopes (1:53, 1:150 and 1:13) and a flat section in the deep end, which simulated the bottom profile at Revere Beach, Massachusetts. The vertical wall was located at the landward end of the 1:13 slope. The solitary waves were generated by a numerical wavemaker located at the opposite end of the vertical wall. Ten capacitance wave gauges were used to measure the wave free-surface elevation. The first four gauges were located in the constant depth region to measure incident wave conditions. Gauges 5, 7, and 9 were located over toes of the slopes, and the remaining gauges 6, 8, and 10 were spaced approximately midway up each slope of the compound beach profile.

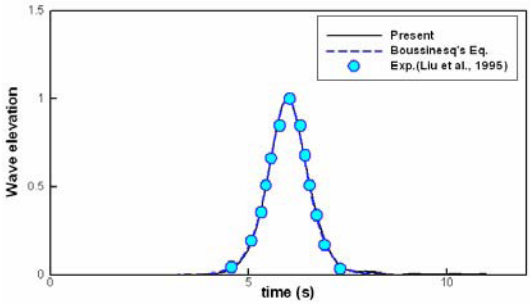

Fig. 1. Comparison of fully developed solitary profiles.

Table 2. Solitary wave parameters.

Case	A_1	A_2	A_3	A_4
A	5.275	1.30	6.26	9.245
B	12.85	2.93	9.42	1.63

Table 3. Condition of simulation.

Case	Δx (cm)	Δy (cm)	Δz (mm)	Δt (sec)
A	5	10	1.1	1/1500
B	4	10	2	1/3000

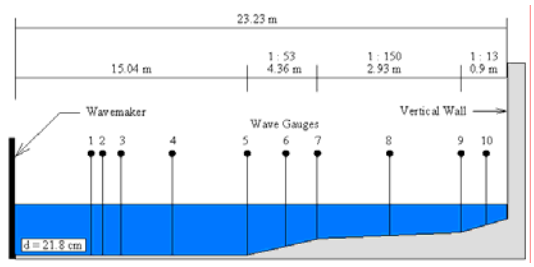

Fig. 2. Schematic view of 2D wave flume and gauge placement.

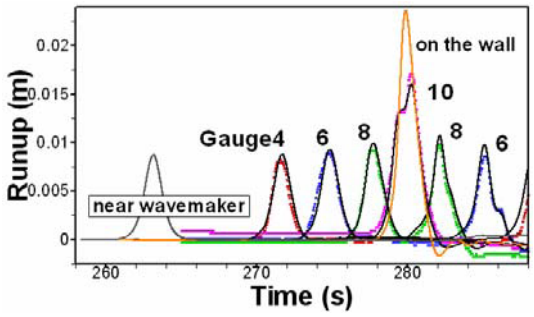

Fig. 3. Time history of solitary run-up in the Case A (—: the simulated results & .....: experiments).

Two solitary wave amplitude ratios are considered in this study. The ratio of initial wave height (η_i) against water depth (d) is $\varepsilon = \eta_i / d$ =0.05 and 0.3 for Cases A and B, respectively. According to the report by Briggs et al. [22], in Case A, neither the incident nor the reflection waves broke, while in Case B, the waves broke at or near the vertical wall, and at the wall the flume of water shot upward, like a jet. The coefficients from Eqs. (14), (15) for solitary waves are listed in Table 2. The simulation parameters listed in Table 3 were chosen after carrying out convergence tests for grid size and time step. For simplicity, in the y-direction, the width of flume is assumed as unit, and ten grids are constantly set at Δy =0.1(m).

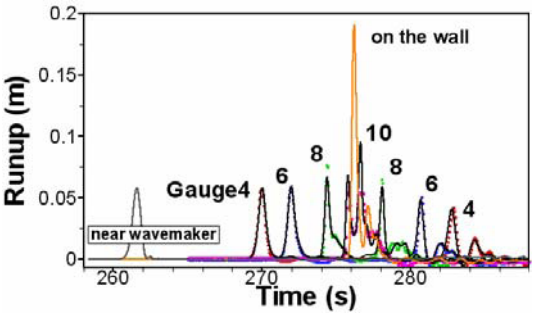

Fig. 4. Time history of solitary run-up in the Case B (—: the simulated results & .....: experiments).

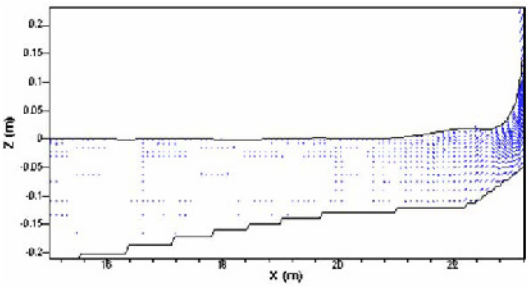

Fig. 5. Typical wave profile and velocity vector of solitary run-up near vertical wall in Case B.

Figs. 3 and 4 present comparisons. For Case A, the numerical results agreed with the experiment. If there were no sloping beach in the flume, the maximum run-up at the vertical wall would be exactly two times the input wave height. In this case, however, the maximum run-up at the vertical wall shows 2.72 times the input wave height because of the shallow water effects from the sloping beach. From the wave profiles in Fig. 3, it can be observed that the solitary wave is reflecting calmly with no wave breaking. Similarly for Case B, the agreement is quite reasonable as compared to the experiment. In particular, the reflected waves from the vertical wall are well simulated, and the non-linear features seem to be stronger than those of Case A. During the convergence tests in Case B, the simulation often diverged when the waves hit the vertical wall. This was because the upward velocity component of the fluid particles increased instantly at that moment, so the time increment, Δt, was not enough to capture the dynamic motions of the fluid. That problem could be fixed by setting a smaller value of Δt. In Fig. 5, the wave behavior near the seawall is nonlinear in accordance with the observation by Briggs et al. [22]. A jet spurts upward at the seawall. When steeper waves than

Table 4. Maximum wave run-up on vertical wall.

Researchers	Max. runup/depth	
	Case A	Case B
Briggs et al. (Experiments)	0.13	2.10
present results	0.124	1.712
Kobayashi & Tega	0.124	0.459
Grilli	0.116	0.435
Kanoglu & Synolakis	0.147	0.881
Takagi	0.101	1.514
Walters	0.106	0.367
Watson et al.	0.132	0.504
Gardarsson	0.110	0.294
Kennedy	0.099	3.564

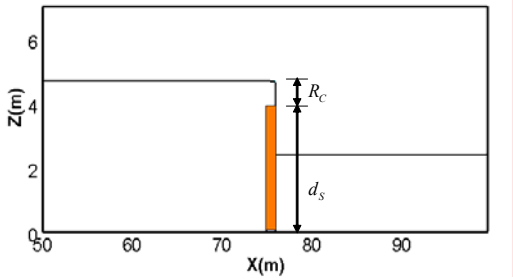

Fig. 6. Initial condition of the free surface profile for open channel flow over a broad-crested weir.

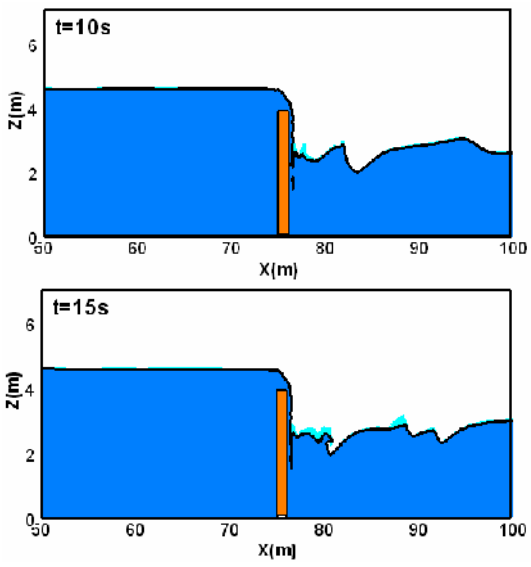

Fig. 7. Free surface profile for open channel flow over a broad-crested weir (R_c =0.8).

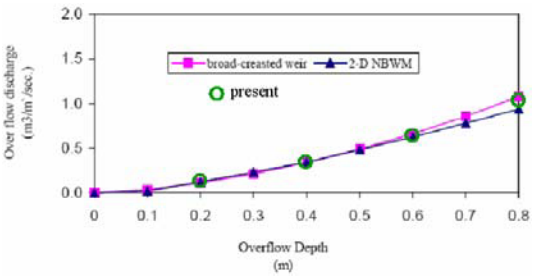

Fig. 8. Comparison of overflow discharge with the weir equation & CFDs.

those of Case B were considered, the breaking phenomenon was accompanied by progressively severe turbulent dissipation. Table 4 lists the maximum run-up values at the vertical wall obtained experimentally by Briggs et al. [22], the present model, and alternative models in the published literature. The present model gives results that are in closer agreement than any of the alternative models quoted.

3.2 Open channel flow over a broad-crested weir

We next consider open channel flow over a broad-crested weir. The upstream level is above the crest level of the weir, and the freeboard (R_c) is negative. For comparison purpose, the following discharge formula expressed by Chadwick and Morfett [23] is used here:

$$q_{weir} = 1.705 \times C_d \left| R_c \right|^{\frac{3}{2}} \tag{16}$$

where C_d is the discharge coefficient and given as

$$C_d = 0.848 C_F \tag{17}$$

$$C_F \cong 0.91 + 0.21\frac{R_c}{B_L} + 0.24\left(\frac{R_c}{R_c + d_s} - 0.35\right) \tag{18}$$

where B_L is the weir width.

Fig. 6 shows the initial condition of the water surface profile. The weir height (d_s) is 4.0m, the weir width is 1.0m, and the freeboard ranges from 0.0 to -0.8m. The total number of grid points is 40,000, and the time increment is 0.0005s.

Fig. 7 shows the overflow over a vertical weir at t=10s and 15s. Fig. 8 shows the comparison to the discharge rate of the weir equation (16) and the simulation results by the 2-D BWNM [24]. It can be seen that the present results agreed well with the weir equation.

Table 5. Geometry of sloping seawalls of slope 1:3 and wave parameters.

Slope	dt (m)	ds (m)	Rc (m)	Hs (m)	T (sec)
1:3	3.0	0.75	0.50	0.95	4.73

Table 6. Comparison between numerical models with the measured dimensionless overtopping discharges.

$Q(10^{-3})$ Saville (exp.)	$Q(10^{-3})$ Amazon	$Q(10^{-3})$ 2-D BWNM	$Q(10^{-3})$ Present
66	39	46	54

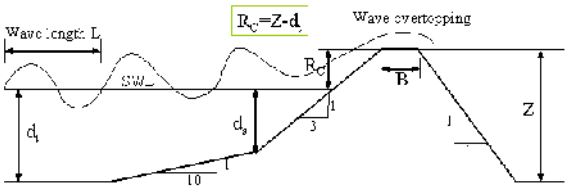

Fig. 9. Sketch explains the case study of regular waves overtopping at sloping seawalls.

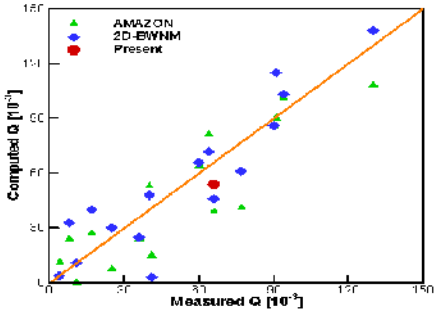

Fig. 10. Comparison between numerical models with the measured dimensionless overtopping discharges.

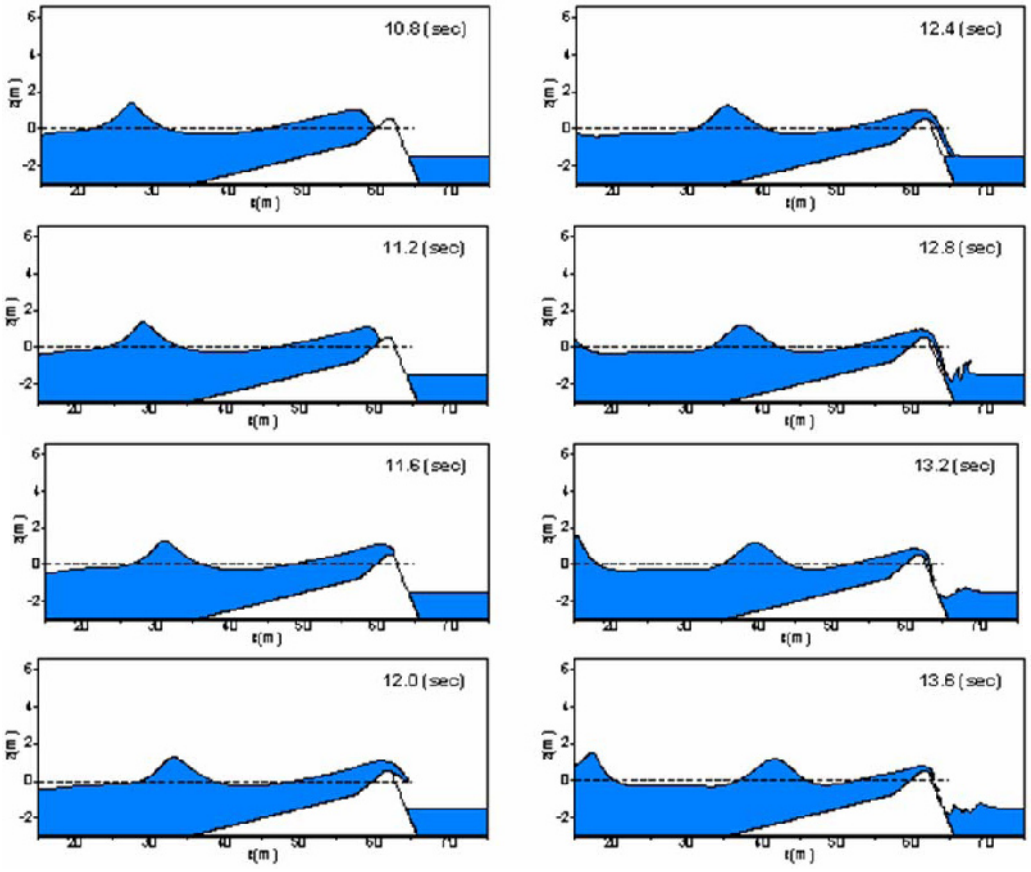

Fig. 11. Time-sequential nonlinear overtopping and overflow motions at the sloping seawall.

3.3 Wave overtopping at sloping seawalls

Regular wave overtopping a sloping seawall of slope 1:3 is simulated. Fig. 9 gives a definition sketch illustrating the geometry of the sloping seawall. The detailed parameters for sloping seawall and regular waves are listed in Table 5.

The comparison between numerical models with the measured dimensionless overtopping discharges, Q, is made in Fig. 10 and Table 6. Here, Q is defined by Hu et al. [7] as

$$Q = \frac{q}{H\sqrt{gH_s}} \tag{19}$$

where q is the non-dimensional average overtopping discharge and g is the gravitational acceleration. An average value of Q is predicted from the time series of overtopping discharge during $4 \le T \le 5$.

From Table 6, the present result is in 82% agreement with the laboratory data, and provides 17% improvement in the performance of the 2-D BWNM [24].

Fig. 11 exhibits the instantaneous free-surface configurations as time sequences. In the figures, we can observe the fully non-linear wave overtopping motions over the sloping seawalls.

4. Concluding remarks

In the present study, the wave run-up and overtopping motions over the coastal structures were numerically simulated by using an LES model, in which the N-S equations are solved with a finite differential algorithm, and the modified MDF technique is employed for solving nonlinear free-surface motions. The present model was applied to the solitary wave run-up on a vertical wall, the overflow simulation without waves at a broad crested weir, and the regular waves overtopping over a sloping seawall. From the all simulated results, the present results agreed well with the laboratory data and improved in performance compared with other numerical results.

Acknowledgment

This research was supported by "Principal Research in Wave Overtopping Power Generation Technology" from the Ministry of Commerce, Industry and Energy.

References

[1] D. H. Peregrine, Long waves on a beach, *J. Fluid Mechanics*, 27 (4) (1967) 815-827.

[2] J. A. Zelt, The run-up of non-breaking and breaking solitary waves, *Coastal Engineering*, 15 (1991) 205-246.

[3] T. V. Karambas and C. Koutitas, A breaking wave propagation model based on the Boussinesq equations. *Coastal Engineering*, 18 (1992) 1-19.

[4] H. A. Schäffer, P. A. Madsen and R. Deigaard, A Boussinesq model for waves breaking in shallow water. *Coastal Engineering*, 20 (1993) 185-202.

[5] B. D. Johnson and N. C. D. T. Kobayashi, Formulation and validation of vertically 2-D shallow-water model, Proc. of 25th Intentional Conference in coastal Engineering, ASCE, (1996) 551-564.

[6] N. Dodd, Numerical model of wave run-up, overtopping, and regeneration, *J. Wateway, Port, Coastal and Ocean Engineering*, 124 (2) (1998) 73-81.

[7] K. Hu, C. G. Mingham and D. M. Causon, Numerical simulation of wave overtopping of coastal structure using the non-linear shallow water equation, *Coastal Engineering*, 41 (2000) 433-465.

[8] C. W. Hirt and B. D. Nichols, Volume of fluid (VOF) method for dynamics of free boundaries, *J. Computational Physics*, 39 (1981) 201-225.

[9] F. C. K. Ting and J. T. Kirby, Dynamics of surf-zone turbulence in a strong plunging breaker, *Coastal Engineering*, 24 (3) (1995) 177-204.

[10] F. C. K. Ting and J. T. Kirby, Dynamics of surf-zone turbulence in a spilling breaker, *Coastal Engineering*, 27 (3) (1996) 131-160.

[11] P. Lin, Numerical modeling of breaking waves. Cornell University, U.S.A, (1998).

[12] P. Lin and P. L. -F. Lui, A numerical study of breaking waves in the surf zone, *J. Fluid Mechanics*, 359 (1998) 239-264.

[13] P. Lin and P. L. -F. Lui, Internal wave-maker for Navier-Stokes equations models, *J. Waterway, Port, Coastal and Ocean Engineering*, 125 (4) (1999) 207-215.

[14] P. L. -F. Liu and P. Lin, Numerical modeling of wave interaction with porous structures, *J. Waterway, Port, Coastal and Ocean Engineering*, 125 (6) (1999) 322-330.

[15] H. Miyata and J. C. Park, Ch. 5 Wave breaking simulation. Potential Flow of Fluids, Computational Mechanics Publications, UK., (1995) 149-176.

[16] J. Smagorinsky, General circulation experiments with the primitive equations. I. The basic experiment, *Monthly Weather Review*, 91 (1963) 99-164.

[17] Y. Takakura, S. Ogawa and T. Ishiguro, Turbulence models for transsonic viscous flow, *AIAA paper*, (1989) No 89-1952CP.

[18] J. C. Park, M. H. Kim and H. Miyata, Fully nonlinear free-surface simulations by a 3D viscous numerical wave tank, *Int. J. for Numerical Methods in Fluids*, 29 (1999) 685-703.

[19] M. Sussman, P. Smereka and S. Osher, A level set approach for computing solutions to incompressible two-phase flow, *J. Computational Physics*, 114 (1994) 272-280.

[20] R. K. C. Chan and R. L. Street, A computer study of finite amplitude water waves, *J. Computational Physics*, 6 (1970) 68-94.

[21] P. L. -F. Liu, Y. S. Cho, M. J. Briggs, U. Kanoglu and C. E. Synolakis, Runup of solitary waves on a circular island, *J. Fluid Mechanics*, 302 (1995) 259-285.

[22] M. Briggs, C. E. Synolakis, U. Kangolu and D. R. Green, Benchmark problem 3: runup of solitary waves on a vertical wall. U.S. Army Engineer Waterways Experiment Station, Vicksburg, MS., (1994).

[23] A. Chadwick and J. Morfett, Hydraulics in civil and environmental engineering. London and New York, E & FN SPON, (1998).

[24] A. Soliman, M. S. Raslan and D. E. Reeve, Numerical simulation of wave overtopping using two dimensional breaking wave model, *Proc. of Coastal Engineering VI*, Cadiz, Spain, (2003) 439-447.